# Elucidation of the Reinforcing Mechanism in Carbon Nanotube/Rubber Nanocomposites

**Fei Deng,[†,‡] Masaei Ito,[§,⊥] Toru Noguchi,[∥] Lifeng Wang,[¶] Hiroyuki Ueki,[∥] Ken-ichi Niihara,[∥] Yoong Ahm Kim,[⊥] Morinobu Endo,[⊥,*] and Quan-Shui Zheng[†,#,*]**

[†]Department of Engineering Mechanics, Tsinghua University, Beijing 100084, China, [‡]Department of Material Science and Engineering, Massachusetts Institute of Technology, Cambridge, Massachusetts 02139, United States, [§]Schlumberger K. K., 2-2-1 Fuchinobe, Sagamihara, Kanagawa 252-0206, Japan, [⊥]Faculty of Engineering, and [∥]Research Center for Exotic Nano Carbon Project, Shinshu University, 4-17-1 Wakasato, Nagano 380-8553, Japan, [¶]Department of Mechanical Engineering, Massachusetts Institute of Technology, Cambridge, Massachusetts 02139, United States, and [#]Center for Nano and Micro Mechanics, Tsinghua University, Beijing 100084, China

**ABSTRACT** High-performance sealants using rubber composites containing multiwalled carbon nanotubes (MWNTs) were developed in order to probe and excavate oil in deeper wells. However, the stress–strain behavior and the reinforcing mechanism of highly concentrated MWNT/rubber composites subjected to large deformation remain largely unexplored. Here we report on the complete stress–strain relationships of MWNT/rubber composites under uniaxial tension before rupture, with a suggestion of a novel reinforcement effect of high concentration of MWNTs. A theoretical model is developed to understand the reinforcing mechanism and estimate the mechanical properties of MWNT/rubber composites under large deformation. We have demonstrated that persistence length and reorientation of MWNTs during stretch have a significant impact on mechanical properties, such as the modulus of the rubber composite. These results provide guidelines for developing MWNT-reinforced composites to achieve desired nonlinear and extreme mechanical performance for a wide range of applications.

**KEYWORDS:** rubber nanocomposites · carbon nanotubes · sealant · mechanical property

Reinforced rubber composites are widely used as sealing materials in reservoir evaluation as well as in oil production under harsh conditions. An excellent sealant material has to have not only sufficient hardness and strength but also appropriate flexibility as well as excellent structural stability under temperatures and pressures such as 175 °C and 135 MPa, typical conditions in present common wells.[1] The demand for oil resources has become one of the main factors threatening the stability of the global economy. Currently, increasing oil exploration and production in much deeper wells is one of the most effective methods to relieve the global energy crisis until the development of a silver bullet in alternative energy.[2] Exploring these deeper areas will demand novel and robust sealant materials for joining adjacent modules consisting of sensors and measurement instruments. Rubber sealants, or O-rings, are especially key components in the exploration and production of oil in deeper wells, which reach high temperature and pressure reservoirs.

To improve durability and strength of rubber materials, extensive use of nanosized filler has been studied since the small size and increased surface area provide improved mechanical properties with low filler loadings. Fillers of various morphologies, including spherical particles such as carbon black[3,4] and silica particles,[5] layers such as clay[6,7] and graphene,[8,9] and carbon nanotube (CNT) fibers such as single-wall or multiwall carbon nanotubes (SWNTs or MWNTs),[10,11] have been adopted as reinforcing material in rubber matrices. Great progress has been made on CNT-reinforced rubber composites because of the high aspect ratio of CNTs as well as their excellent physical properties.[12,13] However, filler dispersion and binding interaction between the matrix and the filler have been seen to seriously influence the mechanical properties of the composite.

Different techniques have been used to attempt to optimize dispersion or bring some adhesion between CNTs and matrices, thus enabling effective stress transfer at the interface. However, the mechanical improvement brought about by incorporation of CNTs remains minor. Recently, Endo *et al.*[1] developed a milling process at low temperature to accomplish the homogeneous dispersion of MWNTs in the matrix rubber and in the future to achieve enhanced elasticity and shear force. Such process allowed us to disperse a high concentration of MWNTs homogeneously within the

* Address correspondence to endo@endomoribu.shinshu-u.ac.jp, zhengqs@tsinghua.edu.cn.

Received for review January 18, 2011 and accepted April 8, 2011.

**Published online April 08, 2011**
**10.1021/nn200201u**

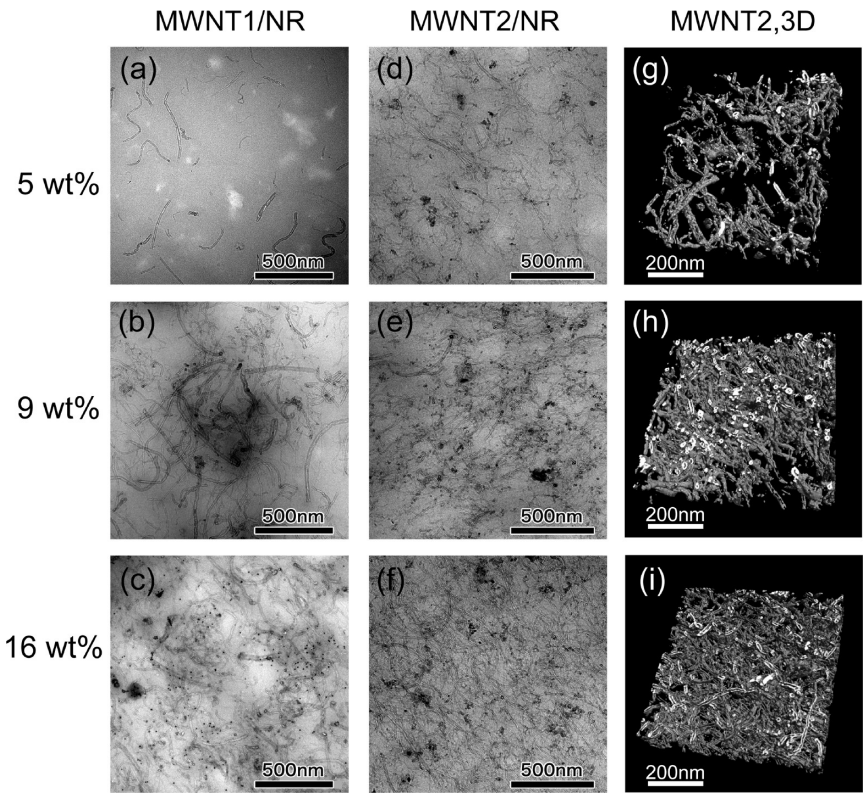


**Figure 1. (a−c) TEM images of the produced MWNT/rubber composites containing 5, 9, and 16 wt % of MWNT1s, respectively. (d−f) TEM images of the produced MWNT/rubber composites containing 5, 9, and 16 wt % MWNT2s, respectively. (g−i) Corresponding 3D images of MWNT2s in 5, 9, and 16 wt % MWNT2/rubber composite. The thickness of each sample is 130 nm.**

rubber matrix and thus to induce cellular structure, thereby resulting in 3 order enhancement of the storage. Moreover, derived O-rings are able to withstand at a 100 °C higher temperature and at a 70 MPa higher pressure, as compared to the currently used O-rings. However, the mechanical properties of such rubber composites as well as the reinforcing mechanism of tubes under larger deformation remain largely unexplored.

In this paper, we investigate the uniaxial tensile large deformation behavior of MWNT/natural rubber (NR) nanocomposites made using an explicit micromechanical model[14] with various volume fractions of MWNTs. Highly nonlinear stress−strain relationships of MWNT/NR composites are obtained up to their respective rupture at tensile strains of 150 to 400%. Furthermore, a theoretical model for MWNT/NR composites is developed to understand the underlying enhancement mechanisms under large deformation; the model indicates that the orientation evolution of MWNTs and the persistence length play a significant role in the macroscopic mechanical response. The predicted stress−strain behaviors using this model agree well with the experimental observations. The model suggests that increasing persistence length of MWNTs is a useful way to enhance the modulus and hardening behavior of rubber composite, which is consistent with the experimental results.

## RESULTS AND DISCUSSION

**Experimental Results.** Two types of typical fillers, MWNT1 with a mean diameter of $d$ = ∼13 nm and length of $L$ = ∼20 $\mu$m and MWNT2 with a mean diameter of $d$ = ∼15 nm and length of $L$ = ∼10 $\mu$m, were prepared by catalytic chemical vapor deposition (CCVD).[15,16] MWNT2s are relatively straighter than MWNT1s. Figure 1a−c shows typical transmission electron microscopy (TEM) images of produced MWNT1s in rubber matrix containing 5, 9, and 16 wt % MWNT1s, respectively. Typical TEM images of the produced MWNT2-filled rubber nanocomposites (Figure 1d−f) depict the tortuous configurations of MWNTs after milling and their homogeneous dispersion in the composites. To further investigate the 3D morphology, the configurations of the MWNT2-filled rubber composite have also been investigated using 3D images with detailed information, as shown in Figure 1g−i, which are obtained by 3D-TEM.[17] It is now evident that the MWNTs formed the 3D network structure in the NR matrix. The MWNT's networks and the interfacial region which would be formed around MWNTs divide the NR matrix into small units, which is like a cellular structure. It assumed that the NR matrix was confined in the cells. The number of the cellular structure increases as the content of the MWNTs increases.

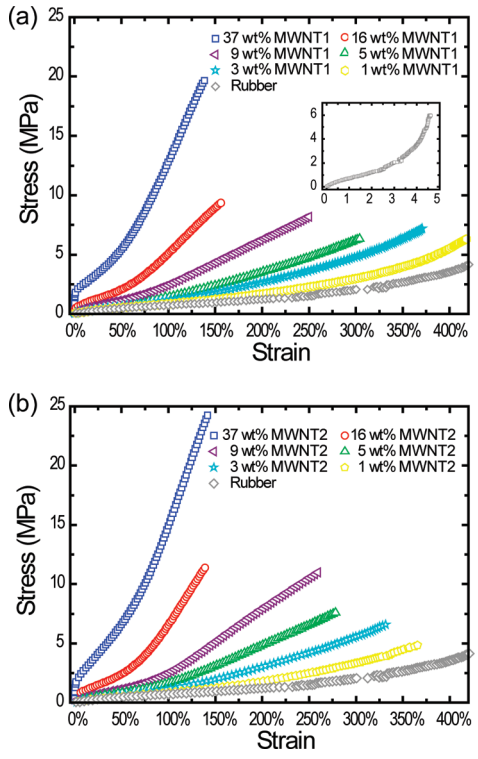


**Figure 2. Experimentally measured stress−strain response of the MWNT/NR composites under uniaxial tension. (a) MWNT1/NR composite and (b) MWNT2/NR composite. The inset in (a) shows a magnified view of NR stress−strain curve.**

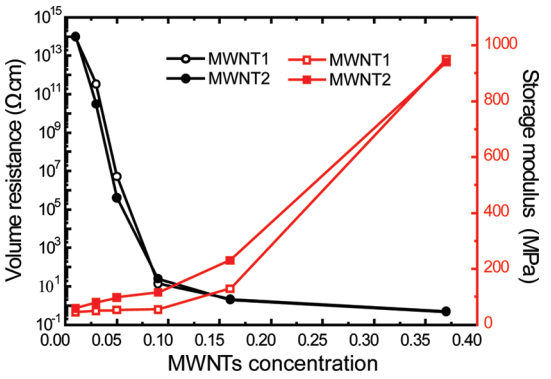


**Figure 3. Experimental results of volume electrical resistance measured at room temperature and the storage modulus for both MWNT1- and MWNT2-filled NR nanocomposites as a function of the concentration of MWNTs.**

Uniaxial tensile testing was conducted on both MWNT1- and MWNT2-filled rubber composites with standard dumbbell #6 test pieces (ISO 37) using a universal testing machine AG-X (SHIMADZU) at an operation temperature of 23 ± 2 °C. The tensile loading speed was 500 ± 50 mm $min^{-1}$. The measured stress−strain curves for these two types of rubber composites with various MWNT concentrations are plotted in Figure 2a,b, respectively. Figure 2 shows an increase of both tangent modulus (the curve slopes) and strength (the stresses at rupture) at a given strain as the weight of MWNTs increases in the composites. The rupture elongations decrease as the weight of MWNTs increases. Note that MWNT2s show comparatively better enhancements than MWNT1s in the composite.

To study the effect of MWNT concentration, the storage modulus was measured by dynamic mechanical analysis (DMA) using equipment SII DMS6100 at room temperature at 1 Hz and strain about 0.1%, per ISO 6721-4. The electrical volume resistance at room temperature was measured using Hiresta-UP for higher than $1 \times 10^6$ Ω·cm per ISO 2951 (dual rings method) and Loresta-GP for lower $1 \times 10^6$ Ω·cm per ISO 2827 (four-point probes method); both pieces of equipment were made by Mitsubishi Chemical Co. for MWNT1 and MWNT2 rubber composites. As expected, the storage modulus for the two types of rubber composites increases as the MWNT concentration increases (Figure 3). For 37 wt % MWNT composites, the storage modulus reaches ~940 MPa, which is about 3 orders of magnitude higher than that of the pure rubber. This trend can also be seen from the initial slope of stress−strain curves in Figure 2a,b. Interestingly, the electrical volume resistance of the composites drops dramatically over 13 orders of magnitude and down to less than 1 Ω·cm as the MWNT concentration increases to 30%. MWNT concentration of 9 to 16 wt % is a transition range in which both the storage modulus and the electrical volume resistance undergo rapid change. This phenomenon was reported before and proposed to be a result of the formation of cellular structures of carbon nanotubes.[1]

Moreover, the tangent modulus of rubber composites changes depending strongly on the applied strain, which can be observed in Figure 2a,b for various MWNT concentrations. When the strain is below 1%, the two MWNT/NR composites have a linear response in the stress−strain curve, showing an increase of tangent modulus for higher MWNT concentrations. When the applied tensile strain reaches a critical point, ~1%, all stress−strain curves yield to a steady value. In other words, the tangent modulus decreases rapidly after this critical strain, which implies that the reinforced cellular structure is followed by a probable network loosening/breakdown process upon stretching.

**Theoretical Model.** As shown in Figures 2 and 3, the cellular structure formed by a MWNT network and occluded NR has a tremendous reinforcement effect on enhancing the storage modulus of NR matrices. However, upon stretching, the tangent moduli for all MWNT/NR nanocomposites of various concentrations in our experiment decrease rapidly over a strain of 1%. We propose that the cellular structure goes through a loosening/breakdown process during stretching and then the main supporting fillers are MWNTs that are highly curved and break away from the network.

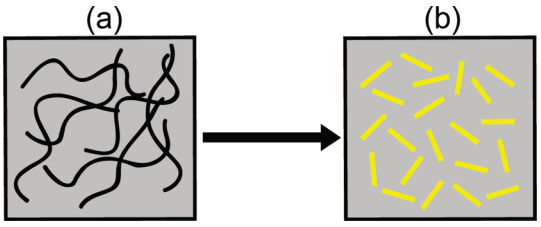


**Figure 4. Schematic of a rubber composite containing randomly dispersed and curved MWNTs, which is equivalent to a rubber composite containing short, straight, and randomly dispersed fiber reinforcements.**

To estimate the effective linear elastic properties of an inclusion/matrix pattern composite, several micromechanical methods have been established with a great success.[18] For strain-related nonlinear elastic properties, these methods are also applicable for estimation of tangent elastic tensors (linear property) based on instantaneous configuration. If filler MWNTs are straight, elastic properties could be obtained by mature micromechanical methods such as interaction direction deviation (IDD)[14] or Mori–Tanaka method.[19] However, as shown in Figure 1, MWNTs as fillers in tested samples are seriously tortuous because of their large aspect ratio (ratio of lengths to diameter), defects, and milling procedures. The tortuous configuration strongly decreases a MWNT's physical properties, such as conductivity[20–22] and elastic modulus.[23] In polymer science, people use persistence length to define the length over which correlations in the direction of the tangent are lost.[24] In consideration that the bending part of MWNTs cannot pass loading efficiently, according to the definition of persistence lengths $l_{sp}$ in polymer science[24] and experimental observation on MWNTs,[25] each long tortuous MWNT is equivalent to several short rigid MWNTs with length $l_{sp}$. Thus the entire composite can be treated as short rigid MWNTs with $l_{sp}$ dispersed randomly in the NR matrix (see Figure 4).

As we know, the elastic properties of a material can be depicted by compliance tensor **S** or stiffness tensor **C**, which link stress and strain with the relationship

$$\varepsilon = \mathbf{S}\sigma, \sigma = \mathbf{C}\varepsilon, \mathbf{S} = \mathbf{C}^{-1} \quad (1)$$

Here, to obtain the elastic compliance/stiffness tensor of the MWNT/NR composite, the IDD estimation[14] is applied because it has an explicit structure and considers the strong interaction between inclusions. Here the effective linear compliance tensor of composite **S*** can be expressed as a function of the aspect ratio and distribution of MWNTs as follows:[14]

$$\mathbf{S}^* = \mathbf{S}_0 + [\mathbf{I} - \int \phi(\psi, \theta, \varphi)\mathbf{H}^d(\psi, \theta, \varphi)\mathbf{C}_0(\mathbf{I} - \Sigma_D(\psi, \theta, \varphi))dg]^{-1}\mathbf{H}^d$$

$$\mathbf{H}^d(\psi, \theta, \varphi) = f((\mathbf{S}(\psi, \theta, \varphi) - \mathbf{S}_0(\psi, \theta, \varphi))^{-1} + \mathbf{C}_0(\mathbf{I} - \Sigma(\psi, \theta, \varphi)))^{-1}$$

$$\mathbf{H}^d = \int \phi(\psi, \theta, \varphi)\mathbf{H}^d(\psi, \theta, \varphi)dg \quad (2)$$

where $\mathbf{C}_0$ and $\mathbf{S}_0$ are the stiffness and compliance tensors of the NR matrix, $\mathbf{S}(\psi, \theta, \varphi)$ and $\mathbf{\Sigma}(\psi, \theta, \varphi)$ are the elastic compliance and Eshelby's tensors of a MWNT, **I** is the fourth-order identity tensor, and $(\psi, \theta, \varphi)$ are the Euler angles.[26] In the integration, $dg = \sin\theta\, d\theta\, d\varphi\, d\psi$, the angle $\theta$ takes value from 0 to $\pi$, $\varphi$ and $\psi$ take value from 0 to $2\pi$, $\mathbf{\Sigma}(\psi,\theta,\varphi)$ and $\mathbf{\Sigma}_D(\psi,\theta,\varphi)$ denote the Eshelby's tensor of MWNTs and their corresponding matrix atmosphere, which reflects the interaction between the MWNTs and the surrounding ones. The Eshelby's tensor of MWNTs is a function of the aspect ratio $p$ (the ratio of $l_{sp}$ to the MWNT diameter $d$) as well as the Poisson's ratio ($\nu_0$) of the matrix material. Replace $p$ with the aspect ratio of matrix atmosphere $q$, and $\mathbf{\Sigma}_D(\psi,\theta,\varphi)$ is obtained. (In this paper, $q$ is adopted as $q = pf^{1/2}$). The detailed form of $\mathbf{\Sigma}(\psi,\theta,\varphi)$ for a $l_{sp}$ long straight MWNT can be found either in Supporting Information or in the literature.[27] The distribution function $\phi(\psi,\theta,\varphi)$ denotes the density of MWNT numbers with Euler angles, and $f$ is the volume fraction of a single MWNT with the persistence length $l_{sp}$. The relationship between volume fraction vol % $f$ in eq 2 and mass fraction wt % $w$ are related as $f = (w/\rho_{MWNT})/(w/\rho_{MWNT} + (1 - w)/\rho_{NR})$, where $\rho_{MWNT}$ and $\rho_{NR}$ are the density of MWNT and NR, respectively.

When stretching the composites in the $x_3$ direction, with other directions of the material remaining free, the strain and stress components in the $x_3$ direction can be expressed as

$$\varepsilon_{33} = S^*_{3333}\sigma_{33} \quad (3)$$

where $(S^*_{3333})^{-1}$ is the tangent modulus $E^*$ (slope ratio of the stress–strain curve) according to instantaneous strain state and structure configuration (dispersion and persistence length of MWNTs). Considering the distribution function and persistence length $l_{sp}$ at each stretching stage, the tangent moduli at different certain strains are obtained. Correspondingly, the stress–strain curve can be predicted, as well, by means of the integral of the tangent moduli on strain.

In eq 2, we treat the mechanical properties of NR in a simple way. Rubber exhibits unique elastic behavior, and it is often modeled as hyperelastic material by various strain energy functions proposed in the literature.[28–32] However, since rubber is comparably very soft with tangent elastic moduli of 6 orders of magnitude smaller than those of MWNTs, the stiffness tensor of the NR is roughly treated to be isotropic, with the Young's modulus equal to the tangent modulus of NR under corresponding uniaxial tensile strain. Moreover, since rubber is almost incompressible (Poisson's ratio $\nu_0 \approx 0.5$), the MWNT/NR composite is also deemed incompressible because the MWNT has much higher stiffness than NR.

The persistence length of the MWNT (corresponding aspect ratio) and the distribution density function $\phi$ are two crucial parameters to the effective elastic

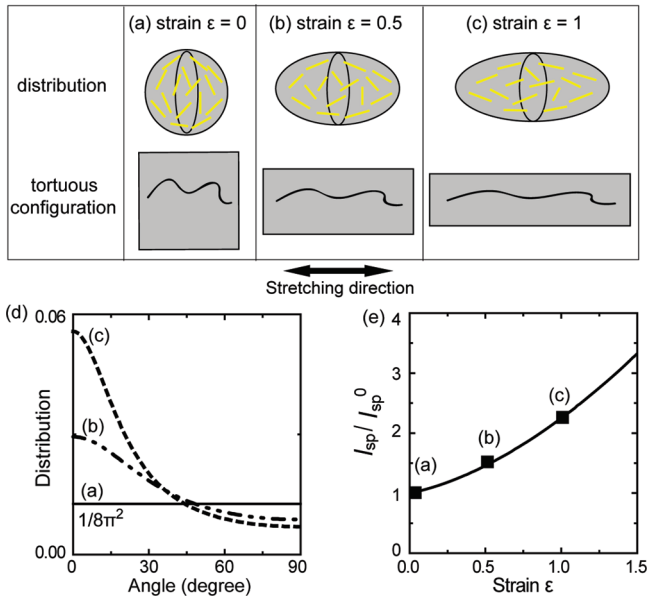


**Figure 5. Nanocomposite model and its characteristic parameters. (a) When the composite is strain-free ($\varepsilon = 0$), randomly dispersed curved MWNTs in the NR matrix are equivalent to short and straight inclusions. When uniaxial stretching is applied to the nanocomposites with (b) 50% and (c) 100% strain, the distribution of MWNTs changes and the resulting orientation of "inclusions" tends to align to the stretching direction. In the meantime, the tortuous configuration of MWNTs is stretched, leading to a change of the persistence length. (d) Distribution as a function of angle between the inclusion and the stretching direction according to eq 4. (e) Corresponding change of $l_{sp}/l_{sp}^0$ as a function of applied strain according to eq 6.**

properties of the MWNT/NR composite in our model. In the undeformed configuration, MWNTs have initial persistence length $l_{sp}^0$ and are randomly dispersed, and upon uniaxial stretching, both persistence length $l_{sp}$ and distribution $\phi$ change with applied strain.

**Effects of Distribution.** Dispersion of fillers has a great influence on property improvement of composites.[33−35] Although MWNTs are distributed randomly in rubber matrix initially, gradual alignment occurs during uniaxial stretching; this stretching must be taken into account in the estimation of the mechanical behavior of the composite. At first, MWNTs in the NR matrix have a great random and uniform dispersion, which is simulated as a unit sphere distribution in the model (see Figure 5a). Then, stretching the composite in the $x_3$ direction up to a strain $\varepsilon$ results in deformation from a unit sphere to a spheroid (Figure 5b,c) with the axial half-axis length of $1 + \varepsilon$ and transverse half-axis length of $(1 + \varepsilon)^{-1/2}$. During this deformation, the randomly dispersed straight MWNTs in the model rotate with a tendency toward the stretching direction (Figure 5a−c). By assuming that the rotations are fully determined by the uniaxial deformation, we can rigorously deduce the distribution density function (Figure 5d) as follows (see Supporting Information):

$$\phi(\theta) = \eta \frac{1}{(1+\varepsilon)^{-1}\cos^2\theta + (1+\varepsilon)^2 \sin^2\theta} \qquad (4)$$

where $\theta$ denotes the angle between the MWNT and the stretching direction, $\eta$ is the normalization coefficient which equals $(1 + \varepsilon)^2 a/(4\pi^2 \ln((1 + a)/(1 - a)))$, $a = (1 - (1 + \varepsilon)^{-3})^{1/2}$. Note that, in the undeformed configuration (strain $\varepsilon = 0$), distribution function $\phi$ is a constant $1/8\pi^2$, which indicates a uniform distribution in space.

**Effects of Persistence Length.** As mentioned before, tortuous configuration will strongly influence the effective elastic properties of MWNTs. Although effective elastic properties of model CNT composites with wavy CNTs, such as sinusoidal,[36] helical,[37] arced, and parabolic[38] CNTs, were studied, the assumed waviness is oversimplified for reasonably modeling the effect of the arbitrary tortuous configurations of the CNTs filler (Figure 1). In fact, a CNT's tortuous configuration is arbitrary, including even with self-entanglement. Thus, rather than waved, the real configurations of CNTs in composites are more similar to those of polymer molecular chains. Indeed, a recent study of Lee *et al.*[25] on the static persistence length of CNTs showed that the root-mean-squared end-to-end distance of tortuous CNTs does follow the same random-coil scaling relation as that for polymer molecular chains. They gave an estimate of the static persistence length $l_{sp}$ of 271 nm for MWNTs with 21 nm diameter and 1−8 $\mu$m length.

The persistence length is a concept in polymer science used to quantify stiffness of a long polymer chain.[24] Formally, the persistence length is defined as the length over which correlations in the direction of the tangent are lost. Informally, for pieces of the polymer which are shorter than the persistence length, the molecule behaves rather like a flexible elastic rod; while for pieces of the polymer that are much longer than the persistence length, the properties can only be

described statistically, like a three-dimensional random walk. In polymer science, it has been widely accepted that polymer molecular chains with lengths shorter than persistence length $l_{sp}$ will behave like straight chains.[39] According to this physical sense, we assume that the contribution of homogeneously dispersed tortuous MWNTs to the effective elastic properties of MWNT/rubber composites can be equivalent to randomly distributed straight MWNTs with the same specific length, the static persistence length $l_{sp}$, whenever the diameters and the total content or weight of the equivalent MWNTs take the same values as those of the real MWNTs. Figure 4 illustrates the equivalent model of the MWNT/rubber composites with the same length $l_{sp}$. With an abundant number of MWNTs with 3D configuration, one can use Lee *et al.*'s method[25] to estimate the static persistence length of MWNTs. Here, we compared the configurations and parameters (diameter and length) of MWNT1s of our sample (5, 9, 16, and 37 wt %) with those in Lee *et al.*'s experiment,[25] and we found they are similar. Thus we took a reasonable estimation of 300 nm for our MWNT1s in the prediction.

During uniaxial stretching, the persistence length of MWNTs changes, as shown schematically in Figure 5a–c. When $L \gg l_{sp}$, following the Karthy–Poroad expression,[40] the mean-squared end-to-end distance $\langle R^2 \rangle$ and CNTs with real lengths $L$ has relation $\langle R^2 \rangle = 2l_{sp}L$. In the stretching process, the original spherical area in the composite turns into an ellipsoid of deformation according to strain $\varepsilon$; thus, the square of the mean end-to-end distance $\langle R^2 \rangle$ becomes

$$\langle R^2 \rangle = \langle R_0^2 \rangle \langle (1+\varepsilon)^2 \cos^2 \theta + (1+\varepsilon)^{-1} \sin^2 \theta \rangle \qquad (5)$$

where $R_0$ is the original squared end-to-end distance. So, the persistence length has form of eq 2. Accordingly, $l_{sp}$ and the tortuous degree of MWNT consequently change with strain $\varepsilon$, as

$$\frac{l_{sp}}{l_{sp}^0} = \frac{1}{2}((1+\varepsilon)^2 + (1+\varepsilon)^{-1}) \qquad (6)$$

where $l_{sp}^0$ is the initial persistence length at zero strain.

As we respectively take into account the persistence length and distribution change during stretching *via* eqs 2–6, we obtain the theoretical predicted stress–strain curve of prepared 37 wt % MWNT/NR composite samples, as shown in Figure 6a. The dotted curve depicts the result considering fixed random distribution and changed persistence length during stretching; the dashed curve depicts the result considering fixed persistence length and changed distribution during stretching; the solid curve indicates the results considering both changes of persistence length and distribution during stretching. It is shown that change of persistence length makes more contribution on elastic stiffness enhancement along with stretching.

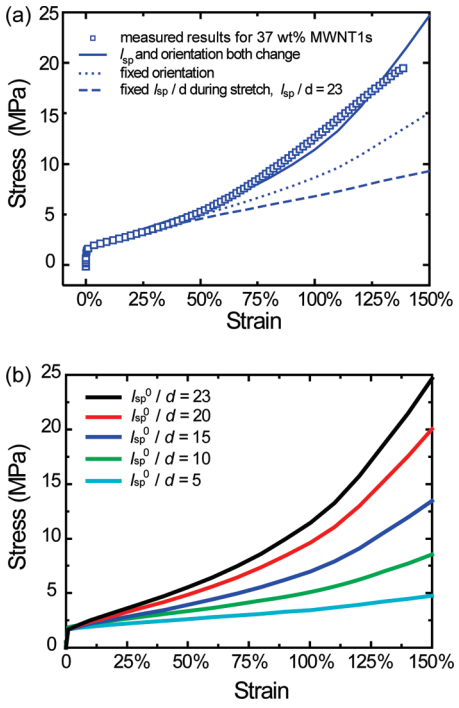


**Figure 6. (a) Contribution of persistence length and distribution to the stress–strain response of MWNT/NR composites. (b) Influence of initial MWNT persistence length on stress–strain response of MWNT/NR composites.**

Changes in persistence length and distribution are determined by the loading method, which is uniaxial stretching in our experiment. With certain loading modes, increasing the initial persistence length can enhance the elastic modulus of a MWNT composite. To investigate the influence of persistence length, predictions on the stress–strain of MWNT/NR composites of various initial MWNTs' persistence length are shown in Figure 6b, with consideration of changes in both MWNT distribution and persistence length.

**Applications of Theoretical Model.** Theoretical stress–strain curves (lines) of a MWNT/NR composite are obtained by comparison with experimental data (scatters) of samples with a series of MWNT concentrations; as shown in Figure 7, these concentrations are 1 wt % (yellow), 3 wt % (cyan), 5 wt % (green), 9 wt % (purple), 16 wt % (red), 37 wt % (blue). Stress and strain in Figure 7 are $\sigma_{33}$ and $\varepsilon_{33}$ in eq 3, respectively. In these theoretical estimates, the rubber's tangent modulus is derived from its uniaxial tensile test (Figure 2a inset) and MWNTs are treated as elastic isotropic with an approximate Young's modulus of 1 TPa and Poisson's ratio of 0.158.[41] As mentioned before, the stress increases dramatically in a very narrow strain region (from 0 to 1%) due to the cellulation structure,[1] and without considering this, our theoretical results start from strain $\varepsilon$ = 1%. Predicted stress–strain results are shown in Figure 7a for MWNT1/NR composites, which agree with experimental data in most strain regions up to 150%, exhibiting highly nonlinear behavior. When

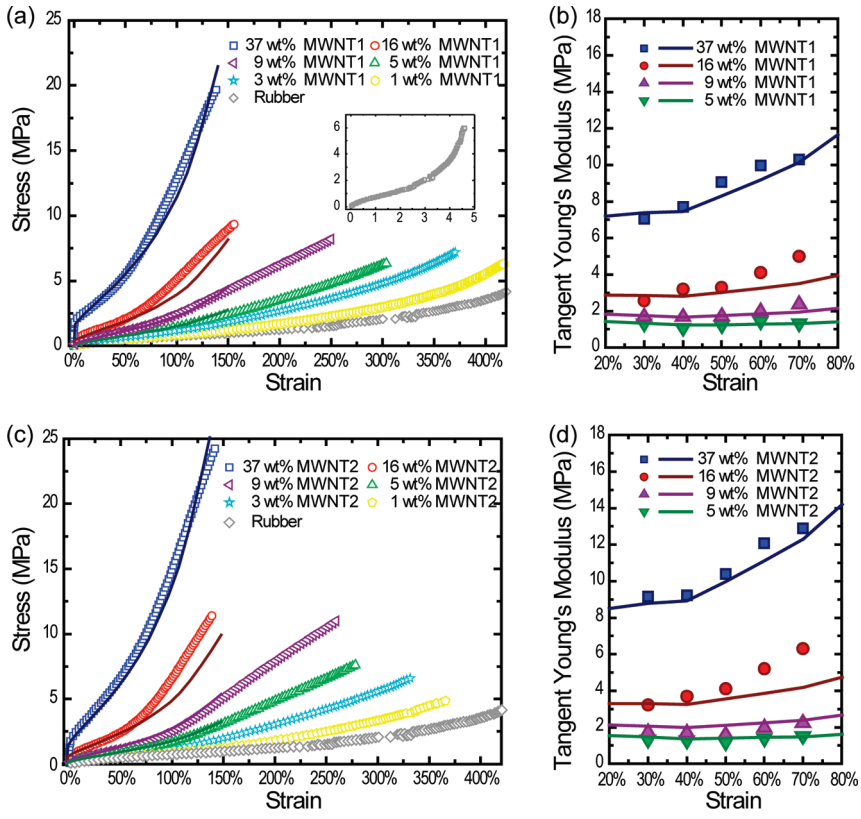


**Figure 7. Comparison between experimental measurements and theoretical predictions for MWNT/NR nanocomposites under uniaxial tension. The symbols are experimental data, and the lines are theoretical predictions. (a) Stress–strain relationship for MWNT1/NR nanocomposites. (b) Tangent modulus for MWNT1/NR nanocomposites at different levels of applied strain. (c) Stress–strain relationship for MWNT2/NR nanocomposites. (d) Tangent modulus for MWNT2/NR nanocomposites at different levels of applied strain.**

the strain is larger than 150%, the assumption $L \gg l_{sp}$ for the derivation of eq 6 is no longer valid.

One serious concern in oil exploration is the tangent modulus of rubber composite at 50% strain (denoted as M50), which is a common working state of O-rings. The predicted tangent modulus at different level of strain is shown in Figure 7b for MWNT1/rubber composite with MWNT concentrations of 5 wt % (green), 9 wt % (purple), 16 wt % (red), and 37 wt % (blue), where measured data are denoted by scatters and prediction by lines. The agreement between our prediction and the experimental data indicates a predictable M50 as a function of MWNT concentration, as also shown Figure 8.

Note that the only parameter adopted in this model is the initial persistence length $l_{sp}^0$, which is examined from TEM images. In section 2.4, we have shown the remarkable influence of MWNT persistence length on elastic modulus and the stress–strain curve of the MWNT/rubber composite. In the interest of further investigating the effect of persistence length, we now look into the measured stress–strain curve for a rubber nanocomposite consisting of MWNT2s. Note that MWNT2s are less curly than MWNT1s from TEM images of MWNT1 and MWNT2 nanocomposites (Figure 1). Since MWNT1s and MWNT2s have similar

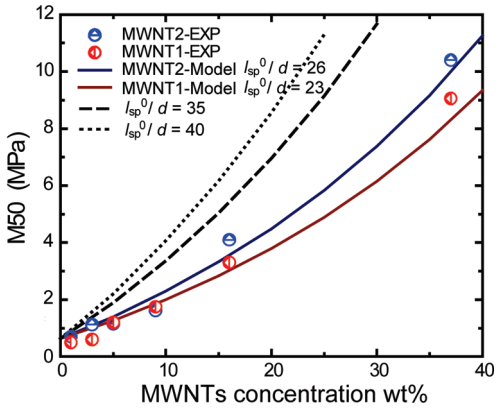


**Figure 8. M50 for MWNT/NR nanocomposites as a function of MWNT concentrations. The symbols are experimental data (1, 3, 5, 9, 16, and 37 wt % of MWNTs); the lines are theoretical predictions. Higher $l_{sp}^0/d$ leads to a higher M50.**

diameter, MWNT2s are considered to have greater persistence length. Thus, MWNT2s have a larger aspect ratio (since aspect ratio $p = l_{sp}/d$). Qualitatively consistent with predictions, both greater tangent modulus and stress are observed for MWNT2/rubber composites compared with those of MWNT1/NR nanocomposites. The longer persistence length of 400 nm is used in the predictions for MWNT2/rubber composites because MWNT2s are straighter. The theoretical stress and

tangent modulus shown in Figure 7c,d for the MWNT2/rubber composite also agree well with experimental data, respectively. MWNT2 enhances the M50 of natural rubber more than MWNT1s do (Figure 8). It also suggested that a larger M50 can be obtained if straighter MWNTs are adopted, as shown in Figure 8 as dashed and dotted lines.

It is also noted that MWNT NR nanocomposites we investigated here are made *via* a milling process at low temperature[1] and have good homogeneous dispersion of MWNTs with only few aggregations/agglomerations. However, usually, filler aggregations/agglomerations formed during preparation would have important influence on elastic properties of the nanocomposite.[42−44] This influence depends on the filler shape, the aggregation/agglomeration degree, and also the geometry of the aggregation/agglomeration. Besides, imperfect interface bonding will reduce the efficiency of load transfer between fillers and matrix and then reduce the effective elastic modulus of the nanocomposite.[42] In the mean time, at the filler−rubber matrix interface, there are complex interactions due to filler and rubber chain interactions, which depend on filler and polymer chemistries, processing details, and physical environments. These interactions might reflect on an interphase region[45,46] or/and might cause agglomerations. Bound rubber interphase serves as an enhancement phase in filler−rubber nanocomposites and will increase the effective stiffness of the composite.[44] Agglomerations, as we mentioned above, will also have an important effect on the elastic properties of the nanocomposite. These above influences need to be taken into account to obtain more accurate theoretical predictions for nanocomposites exhibiting aggregation/agglomeration, interphase and imperfect interface.

## CONCLUSIONS

In summary, we have reported experimentally and theoretically on the nonlinear stress−strain response of two types of MWNT/NR composites under large tensile deformation. Experimental study has shown both tangent modulus and strength increase with more filler MWNTs in the composites, resulting in a reduction of rupture elongations. Study of the strengthening mechanism of MWNT/NR composites is explored to show that the persistence length of tortuous MWNTs and the orientation evolution of MWNTs upon stretching play a key role in the enhancement. Theoretical predictions based on this mechanism are in excellent agreement with experimental data of the stress−strain response up to 150% strain. These results indicate the use of more straight MWNTs with longer persistence lengths can remarkably enhance the elastic property of the composites. Furthermore, a critical tensile strain was found, after which the tangent modulus decreases dramatically, implying the internal structural change of the MWNT network, such as the partial network looseness and cellulation breach. This suggests a possible way to enhance the strength of MWNT/rubber composites by improving the cross-linking of the carbon-tube network. These results provide guidelines for future design and innovation of CNT/rubber composites with optimized mechanical performance.

## METHODS

**Preparation of Rubber Nanocomposites.** Composite material with 100 g of NR (CV-60) and 5, 10, 20, and 60 g of respective fillers was prepared by CCVD. The corresponding mass concentrations are 5, 9, 16, and 37 wt %. The density of NR and MWNTs prepared are ∼0.93 and ∼2.0 g cm$^{-3}$, respectively. The respective compounds were then tight-milled five times with the nip gap of 0.2 mm. To prepare noncured specimens, the compounds were sheeted into a thickness of 1.2 mm and pressed for 2 min at 100 °C to form 1 mm thick sheets. For cured composite specimens, 2 phr of peroxide was added (2 g of peroxide added to 100 g of specimens), and the compounds were likewise sheeted into a thickness of 1.2 mm and press-cured for 20 min at 165 °C to form 1 mm thick sheets.

The ultrathin sections were prepared by a focused ion beam (FIB) at cryogenic temperature (−120 °C).[47] The TEM and 3D-TEM experiments were carried out on a JEM-2200FS (JEOL Co., Ltd., Japan) operated at 200 kV and equipped with a slow-scan CCD camera (Gatan USC1000, Gatan Inc.) as the detector. Detailed experimental protocol can be found elsewhere.[17]

*Acknowledgment.* Financial support from the National Natural Science Foundation of China Grants 10672089, 10772100, and 10832005 and from the China 973 Program Grants 2007*CB*936803 is gratefully acknowledged. This work was also partially supported by NEDO (New Energy and Industrial Technology Development Organization), METI (Ministry of Economy, Trade and Industry), Exotic Nanocarbons, Japan Regional Innovation Strategy Program by the Excellence, JST (Japan Science and Technology Agency), and MEXT (Ministry of Education, Culture, Sports, Science and Technology) in Japan.

*Supporting Information Available:* Additional derivation details and equations. This material is available free of charge *via* the Internet at http://pubs.acs.org.

## REFERENCES AND NOTES

1. Endo, M.; Noguchi, T.; Ito, M.; Takeuchi, K.; Hayashi, T.; Kim, Y. A.; Wanibuchi, T.; Jinnai, H.; Terrones, M.; Dresselhaus, M. S. Extreme-Performance Rubber Nanocomposites for Probing and Excavating Deep Oil Resources Using Multi-Walled Carbon Nanotubes. *Adv. Funct. Mater.* **2008,** *18*, 3403–3409.
2. McKinsey&Company, McKinsey Conversations with Global Leaders: Andrew Gould of Schlumberger; *McKinsey Quarterly*, April, 2010.
3. Rigbi, Z. Reinforcement of Rubber by Carbon-Black. *Adv. Polym. Sci.* **1980,** *36*, 21–68.
4. Kraus, G. Reinforcement of Elastomers by Carbon-Black. *Angew. Makromol. Chem.* **1977,** *60*, 215–248.
5. Wolff, S. Chemical Aspects of Rubber Reinforcement by Fillers. *Rubber Chem. Technol.* **1996,** *69*, 325–346.

6. Wang, Y. Z.; Zhang, L. Q.; Tang, C. H.; Yu, D. S. Preparation and Characterization of Rubber–Clay Nanocomposites. *J. Appl. Polym. Sci.* **2000,** *78*, 1879–1883.
7. Rezende, C. A.; Braganca, F. C.; Doi, T. R.; Lee, L. T.; Galembeck, F.; Boue, F. Natural Rubber–Clay Nanocomposites: Mechanical and Structural Properties. *Polymer* **2010,** *51*, 3644–3652.
8. Kim, H.; Abdala, A. A.; Macosko, C. W. Graphene/Polymer Nanocomposites. *Macromolecules* **2010,** *43*, 6515–6530.
9. Cai, D. Y.; Song, M. Recent Advance in Functionalized Graphene/Polymer Nanocomposites. *J. Mater. Chem.* **2010,** *20*, 7906–7915.
10. Baughman, R. H.; Zakhidov, A. A.; de Heer, W. A. Carbon Nanotubes—The Route toward Applications. *Science* **2002,** *297*, 787–792.
11. Dresselhaus, M. S.; Dresselhaus, G.; Eklund, P. C. *Science of Fullerenes and Carbon Nanotubes*; Academic Press: San Diego, CA, 1996.
12. Gogotsi, Y. High-Temperature Rubber Made from Carbon Nanotubes. *Science* **2010,** *330*, 1332–1333.
13. Wong, E. W.; Sheehan, P. E.; Lieber, C. M. Nanobeam Mechanics: Elasticity, Strength, and Toughness of Nanorods and Nanotubes. *Science* **1997,** *277*, 1971–1975.
14. Zheng, Q. S.; Du, D. X. An Explicit and Universally Applicable Estimate for the Effective Properties of Multiphase Composites Which Accounts for Inclusion Distribution. *J. Mech. Phys. Solids* **2001,** *49*, 2765–2788.
15. Endo, M. Grow Carbon-Fibers in the Vapor-Phase. *CHEMTECH* **1988,** *18*, 568–576.
16. Endo, M.; Kim, Y. A.; Hayashi, T.; Nishimura, K.; Matusita, T.; Miyashita, K.; Dresselhaus, M. S. Vapor-Grown Carbon Fibers (VGCFs): Basic Properties and Their Battery Applications. *Carbon* **2001,** *39*, 1287–1297.
17. Jinnai, H.; Spontak, R. J.; Nishi, T. Transmission Electron Microtomography and Polymer Nanostructures. *Macromolecules* **2010,** *43*, 1675–1688.
18. Milton, G. W. *The Theory of Composites*; Cambridge University Press: New York, 2002.
19. Mori, T.; Tanaka, K. Average Stress in Matrix and Average Elastic Energy of Materials with Misfitting Inclusions. *Acta Metall.* **1973,** *21*, 571–574.
20. Deng, F.; Zheng, Q. S. An Analytical Model of Effective Electrical Conductivity of Carbon Nanotube Composites. *Appl. Phys. Lett.* **2008,** *92*, 071902.
21. Deng, F.; Zheng, Q. S.; Wang, L. F.; Nan, C. W. Effects of Anisotropy, Aspect Ratio, and Nonstraightness of Carbon Nanotubes on Thermal Conductivity of Carbon Nanotube Composites. *Appl. Phys. Lett.* **2007,** *90*, 021914.
22. Song, P. C.; Liu, C. H.; Fan, S. S. Improving the Thermal Conductivity of Nanocomposites by Increasing the Length Efficiency of Loading Carbon Nanotubes. *Appl. Phys. Lett.* **2006,** *88*, 153111.
23. Andrews, R.; Weisenberger, M. C. Carbon Nanotube Polymer Composites. *Curr. Opin. Solid State Mater. Sci.* **2004,** *8*, 31–37.
24. Flory, P. J. *Principles of Polymer Chemistry*; Cornell University Press: Ithaca, NY, 1971.
25. Lee, H. S.; Yun, C. H.; Kim, H. M.; Lee, C. J. Persistence Length of Multiwalled Carbon Nanotubes with Static Bending. *J. Phys. Chem. C* **2007,** *111*, 18882–18887.
26. Huang, M. Perturbation Approach to Elastic Constitutive Relations of Polycrystals. *J. Mech. Phys. Solids* **2004,** *52*, 1827–1853.
27. Mura, T. *Micromechanics of Defects in Solids*; Martinus Nijhoff: Dordrecht, The Netherlands, 1987.
28. Boyce, M. C.; Arruda, E. M. Constitutive Models of Rubber Elasticity: A Review. *Rubber Chem. Technol.* **2000,** *73*, 504–523.
29. Ogden, R. W. Large Deformation Isotropic Elasticity - Correlation of Theory and Experiment for Incompressible Rubberlike Solids. *Proc. R. Soc. London, Ser. A* **1972,** *326*, 565.
30. Rivlin, R. S. Large Elastic Deformations of Isotropic Materials 0.1. Fundamental Concepts. *Philos. Trans. R. Soc. London, Ser. A* **1948,** *240*, 459–508.
31. Rivlin, R. S. Large Elastic Deformations of Isotropic Materials 0.3. Some Simple Problems in Cylindrical Polar Coprdinates. *Philos. Trans. R. Soc. London, Ser. A* **1948,** *240*, 509–525.
32. Yeoh, O. H. Characterization of Elastic Properties of Carbon-Black-Filled Rubber Vulcanizates. *Rubber Chem. Technol.* **1990,** *63*, 792–805.
33. Cheng, Q. F.; Bao, J. W.; Park, J.; Liang, Z. Y.; Zhang, C.; Wang, B. High Mechanical Performance Composite Conductor: Multi-walled Carbon Nanotube Sheet/Bismaleimide Nanocomposites. *Adv. Funct. Mater.* **2009,** *19*, 3219–3225.
34. Ji, Y.; Huang, Y. Y.; Rungsawang, R.; Terentjev, E. M. Dispersion and Alignment of Carbon Nanotubes in Liquid Crystalline Polymers and Elastomers. *Adv. Mater.* **2010,** *22*, 3436–3440.
35. Zhao, Y.; Barrera, E. V. Asymmetric Diamino Functionalization of Nanotubes Assisted by BOC Protection and Their Epoxy Nanocomposites. *Adv. Funct. Mater.* **2010,** *20*, 3039–3044.
36. Fisher, F. T.; Bradshaw, R. D.; Brinson, L. C. Fiber Waviness in Nanotube-Reinforced Polymer Composites-1: Modulus Predictions Using Effective Nanotube Properties. *Compos. Sci. Technol.* **2003,** *63*, 1689–1703.
37. Shi, D. L.; Feng, X. Q.; Huang, Y. G. Y.; Hwang, K. C.; Gao, H. J. The Effect of Nanotube Waviness and Agglomeration on the Elastic Property of Carbon Nanotube-Reinforced Composites. *J. Eng. Mater. Technol.* **2004,** *126*, 250–257.
38. Shao, L. H.; Luo, R. Y.; Bai, S. L.; Wang, J. Prediction of Effective Moduli of Carbon Nanotube-Reinforced Composites with Waviness and Debonding. *Compos. Struct.* **2009,** *87*, 274–281.
39. Chaikin, P. M.; Lubensky, T. C. *Principles of Condensed Matter Physics*; Cambridge University Press: New York, 1995.
40. Kratky, O.; Porod, G. Rontgenuntersuchung Geloster Fadenmolekule. *Recl. Trav. Chim. Pays-Bas* **1949,** *68*, 1106–1122.
41. Wang, L. F.; Zheng, Q. S.; Liu, J. Z.; Jiang, Q. Size Dependence of the Thin-Shell Model for Carbon Nanotubes. *Phys. Rev. Lett.* **2005,** *95*, 105501.
42. Barai, P.; Weng, G. J. A Theory of Plasticity for Carbon Nanotube Reinforced Composites. *Int. J. Plast.* **2011,** *27*, 539–559.
43. Deng, F.; Van Vliet, K. J. Prediction of Elastic Properties for Polymer–Particle Nanocomposites Exhibiting an Interphase. *Nanotechnology* **2011,** *22*, 165703.
44. Qu, M.; Deng, F.; Kalkhoran, S. M.; Gouldstone, A.; Robisson, A.; Van Vliet, K. J. Nanoscale Visualization and Multiscale Mechanical Implications of Bound Rubber Interphases in Rubber–Carbon Black Nanocomposites. *Soft Matter* **2011,** *7*, 1066–1077.
45. Drzal, L. T. The Role of the Fiber Matrix Interphase on Composite Properties. *Vacuum* **1990,** *41*, 1615–1618.
46. Stickney, P. B.; Falb, R. D. Carbon Black–Rubber Interactions and Bound Rubber. *Rubber Chem. Technol.* **1964,** *37*, 1299–1340.
47. Niihara, K.; Kaneko, T.; Suzuki, T.; Sato, Y.; Nishioka, H.; Nishikawa, Y.; Nishi, T.; Jinnai, H. Nanoprocessing and Nanofabrication of a Structured Polymer Film by the Focused-Ion-Beam Technique. *Macromolecules* **2005,** *38*, 3048–3050.